5. Blanks, R. F., and J. M. Prausnitz, *Ind. Eng. Chem. Fundamentals*, **3**, 1 (1964).
6. Burrell, H., *Interchem. Rev.*, **14**, 3, 31 (1955).
7. Booth, C., G. Gee, G. Holden, and G. R. Williamson, *Polymer*, **5**, 343 (1964).
8. Brown, W. B., G. Gee, and W. D. Taylor, *ibid.*, 362.
9. Conway, B. E., and M. L. Lakhanpal, *J. Polymer Sci.*, **46**, 75, 93 (1960).
10. Flory, P. J., "Principles of Polymer Chemistry," Cornell Univ. Press, New York (1953).
11. Flory, P. J., *J. Chem. Phys.*, **10**, 51 (1942).
12. *Ibid.*, **9**, 660 (1941).
13. Flory, P. J., and W. R. Krigbaum, *ibid.*, **18**, 1086 (1950).
14. ———, *Ann. Rev. Phys. Chem.*, **2**, 383 (1951).
15. Guggenheim, E. A., "Mixtures," Oxford Press, London (1952).
16. Heil, J. F., Doctoral dissertation, Univ. California, Berkeley (1965).
17. Hildebrand, J. H., and R. L. Scott, "The Solubility of Non-electrolytes," Reinhold, New York (1950).
18. Huggins, M. L., *J. Am. Chem. Soc.*, **86**, 3535 (1964).
19. ———, "Physical Chemistry of High Polymers," Wiley, New York (1958).
20. ———, *Ann. N. Y. Acad. Sci.*, **43**, 1 (1942).
21. ———, *J. Chem. Phys.*, **9**, 440 (1941).
22. Krigbaum, W. R., and D. O. Geymer, *J. Am. Chem. Soc.*, **81**, 1859 (1959).
23. Malcolm, G. N., and J. S. Rowlinson, *Trans. Faraday Soc.*, **53**, 921 (1957).
24. Moore, W. R., and R. Shuttleworth, *J. Polymer Sci.*, Pt. A, **1**, 733 (1963).
25. Münster, A., "Statistische Thermodynamik," Springer-Verlag, Berlin (1956).
26. Prigogine, I., "The Molecular Theory of Solution," Interscience, New York (1957).
27. Scatchard, G., *Chem. Rev.*, **8**, 321 (1931).
28. Schulz, G. V., and B. Jirgenson, *Z. Phys. Chem.*, **B46**, 105 (1940).
29. Stuart, H. A., "Die Physik der Hochpolymeren," Vol. II, Springer Verlag, Berlin (1956).
30. Tompa, H., *J. Polymer Sci.*, **8**, 51 (1952).
31. ———, "Polymer Solutions," Academic Press, New York (1956).
32. Van Laar, J. J., *Z. Phys. Chem.*, **72**, 723 (1910).
33. Wilson, G. M., *J. Am. Chem. Soc.*, **86**, 127 (1964).
34. Yamakawa, H., S. A. Rice, R. Corneliussen, and L. Kotin, *J. Chem. Phys.*, **38**, 1759 (1963).

Manuscript received November 16, 1965; revision received February 7, 1966; paper accepted February 8, 1966.

Reduction of Single Particles and Packed Beds of Hematite with Carbon Monoxide

M. A. OSMAN, F. S. MANNING, and W. O. PHILBROOK

Carnegie Institute of Technology, Pittsburgh, Pennsylvania

Sintered spheres of reagent grade hematite and particles of vermilion ore were reduced by carbon monoxide-carbon dioxide mixtures over the temperature range 820° to 920°C. If all the weight loss were assumed to occur at a single hematite-iron interface, then the early stages of reduction could be correlated by a series combination of the individual resistances due to boundary-layer transport, transport through the reduced iron shell, and interfacial chemical reaction. Sintering and cracking affected the reduction at later stages. Particle reducibility, measured as rate of weight loss, was independent of particle porosity.

Packed beds of similar sized vermilion ore particles were reduced with carbon monoxide-carbon dioxide mixtures at temperatures between 820° and 920°C. Barner's and Spitzer's methods of estimating fixed-bed reduction rates and exit gas compositions were modified to include the multiple-step, single-particle kinetic models. The resulting predictions of fractional reduction agreed closely with the present data; however, theoretical and experimental exit gas compositions differed considerably.

Due to the great industrial importance of pig iron production, there is intense economic interest both in optimizing current iron ore reduction processes, for example, blast furnaces, and in developing more economical reduction and smelting techniques. Often, reduction of iron ore lumps with hot reducing gases containing carbon monoxide, carbon dioxide, hydrogen, and water is involved.

The present work had three goals. First, single-particle reduction data were taken in order to elucidate the roles played by industrially controllable variables such as reduction temperature, reducing gas composition, and intraparticle porosity. Second, isothermal reduction runs were made with fixed beds of vermilion ore particles. A better understanding of fixed-bed reduction was desired as a step toward evaluating the considerable economic potential to be gained by optimizing the temperature, flow rate, and composition of the reducing gas and the size, porosity, and

M. A. Osman's present address is 16 Menes Street, Heliopolis, Cairo, Egypt.

composition of the ore particles or agglomerates. Finally, the above data were used to improve Barner's and Spitzer's methods (*12, 17*) of predicting packed-bed reduction rates from single particle kinetics.

THEORY

Hougen's model (*8*) of gas-solid reaction is applied to reduction of single hematite spheres and the resulting mathematical rate expressions are presented. Finally, Barner's (*1, 2*) and Spitzer's (*17*) models of fixed-bed reduction are summarized.

Single-Particle Reduction

The heterogeneous reaction:

$$Fe_2O_3\ (s) + 3\ CO\ (g) \rightleftharpoons 2\ Fe\ (s) + 3\ CO_2\ (g)$$

involves the following steps:

1. Transfer of reactant gas from the bulk gas stream through the gas boundary layer to the exterior particle surface and the reverse transfer of the product gas.
2. Inward diffusion of reducing gas and outward diffusion of product gas across the reduced outer shell to the interior unreacted core surface.
3. Chemical reaction at the interface between the reacted outer shell and the unreacted inner core.

The specific case of hematite reduction to iron involves the successive reactions $Fe_2O_3 \rightarrow Fe_3O_4 \rightarrow FeO \rightarrow Fe$ if the reaction occurs at temperatures above 560°C. Below 560°C. the reduction proceeds as $Fe_2O_3 \rightarrow Fe_3O_4 \rightarrow Fe$. At present, the additional complexities due to varying physical properties and inhomogeneities in the ore are usually neglected. When a partially reduced hematite pellet is split (*4, 6, 13* to *15*) concentric shells of all lower oxide phases are usually observed. The magnetite and wüstite layers are often quite thin.

Hougen's (*8*) model can be applied to hematite reduction if the following additional assumptions are made:

1. Thicknesses of the magnetite and wüstite layers are neglected, thus reducing the system to a hematite core surrounded by an iron shell.
2. All oxygen removal, and consequently the entire weight loss, occurs at the wüstite-iron interface.
3. The spherical shape of the particle and the spherical symmetry of the reduction process remain unchanged during reduction, that is, no cracking and/or sintering.

Mathematical description is further facilitated by assuming that (1) reduction proceeds isothermally, and (2) reduction is pictured as being quasi steady state.

Hematite reduction rates may be defined by

$$-\frac{dn_{Fe_2O_3}}{dt} = -\frac{1}{3}\frac{dn_{CO}}{dt} = +\frac{1}{2}\frac{dn_{Fe}}{dt} = +\frac{1}{3}\frac{dn_{CO_2}}{dt} \tag{1}$$

or by the weight loss, that is, the oxygen removed:

$$\frac{dW_O}{dt} = \left(\frac{-48\ \text{g. O}}{\text{mole } Fe_2O_3}\right)\left(\frac{dn_{Fe_2O_3}}{dt}\right) = \left(\frac{-16\ \text{g. O}}{\text{mole CO}}\right)\left(\frac{dn_{CO}}{dt}\right) = \left(\frac{+16\ \text{g. O}}{\text{mole } CO_2}\right)\left(\frac{dn_{CO_2}}{dt}\right) \tag{2}$$

or by the rate at which the unreduced core radius recedes:

$$\frac{dW_O}{dt} = -d_O\,(4\pi x_i^2)\left(\frac{dx_i}{dt}\right) \tag{3}$$

Hematite reduction has now been simplified to three distinct processes: boundary-layer transport, mass transfer through the reduced shell, and chemical reaction at the oxide-metal interface. These processes may now be described mathematically for the special case of a binary mixture of carbon monoxide-carbon dioxide as the reducing gas.

Inward gas transfer:

$$-\frac{dW_O}{dt} = \left(\frac{-16\ \text{g. O}}{\text{mole CO}}\right) h\,4\pi x_o^2\,P(y_f' - y_o') \tag{4}$$

Inward gas diffusion:

$$-\frac{dW_O}{dt} = \left(\frac{-16\ \text{g. O}}{\text{mole CO}}\right)\frac{D_{eff}\,P}{\mathcal{R}\,T}\,4\pi x_o x_i\left(\frac{y_o' - y_i'}{x_o - x_i}\right) \tag{5}$$

Chemical reaction:

$$-\frac{dW_O}{dt} = \left(\frac{-16\ \text{g. O}}{\text{atom O}}\right) k\,4\pi x_i^2\,P(y_i' - y_i''/K_e) \tag{6}$$

Outward gas diffusion:

$$-\frac{dW_O}{dt} = \left(\frac{16\ \text{g. O}}{\text{mole } CO_2}\right)\frac{D_{eff}P}{\mathcal{R}\,T}\,4\pi x_o x_i\frac{y_o'' - y_i''}{x_o - x_i} \tag{7}$$

Outward gas transfer:

$$-\frac{dW_O}{dt} = \left(\frac{16\ \text{g. O}}{\text{mole } CO_2}\right) h\,4\pi x_o^2\,P(y_f'' - y_o'') \tag{8}$$

By combining these individual resistances in series and by using Equation (3) one obtains

$$-\frac{(d_O/16)x_i^2}{P}\frac{dx_i}{dt}\left\{\left\{\frac{1}{h\,x_o^2} + \frac{x_o - x_i}{\frac{D_{eff}}{\mathcal{R}\,T}x_o x_i}\right\}\left(1 + \frac{1}{K_e}\right) + \frac{1}{k\,x_i^2}\right\} = y_f' - \frac{y_f''}{K_e} \tag{9}$$

Integration of Equation (9) for the special case of negligible accumulation of carbon dioxide in the bulk gas phase yields

$$\frac{Pt}{d_O x_o} = \frac{1 - \frac{x_i}{x_o}}{k} + \left(1 + \frac{1}{K_e}\right)\left[\frac{1 - \left(\frac{x_i}{x_o}\right)^3}{3h} + \frac{x_o\left\{1 - 3\left(\frac{x_i}{x_o}\right)^2 + 2\left(\frac{x_i}{x_o}\right)^3\right\}}{6\,(D_{eff}/\mathcal{R}T)}\right] \tag{10}$$

Various simplifications of this general model may be obtained by assuming which resistance(s) controls the overall rate. A brief summary of prior use of these simplifications to correlate data now follows.

Kawasaki et al. (*9*) concluded that the reduction rate of porous hematite pellets with carbon monoxide and hydrogen, in the temperature range of 850° to 1,120°C., was controlled by the gaseous diffusion through the boundary layer and the reduced iron shell.

McKewan (*13, 14*), using both carbon monoxide and hydrogen, has shown that the reduction of hematite spheres can be described by surface reaction mechanism which may be obtained from Equation (10) by neglecting the boundary-layer transport and the shell diffusion terms.

$$\frac{48\,k\,Pt}{x_o\,d_O} = \left(1 - \frac{x_i}{x_o}\right) = 1 - (1 - R)^{1/3} \tag{11}$$

McKewan (*13, 14*) reported that reduction by carbon monoxide at 760°C. was characterized by a high initial rate which decreased slowly with time until the pellet

was reduced approximately 30%. The rate thereafter remained constant up to 70% reduction. However, at a higher temperature of 1,120°C. the observed rate remained substantially constant. McKewan reported an activation energy of 8.5 kcal./mole for reduction of hematite spheres with carbon monoxide.

Themelis and Gauvin (*19*) correlated within ± 30% deviation the data of fifteen investigators on the reduction of hematite ores with carbon monoxide and hydrogen. They used the single-step surface reaction mechanism. Both hydrogen and carbon monoxide reduction exhibited an activation energy of 4.2 kcal./mole but reduction by hydrogen was approximately six times faster than by carbon monoxide.

If boundary-layer transport offers negligible resistance, then Equation (11) simplifies to

$$\frac{16\,P\,t}{d_O\,x_o} = \frac{1-\left(\frac{x_i}{x_o}\right)}{k} + \left(1+\frac{1}{K_e}\right) \left[\frac{x_o\left\{1-3\left(\frac{x_i}{x_o}\right)+2\left(\frac{x_i}{x_o}\right)^3\right\}}{6(D_{\text{eff}}/\mathcal{R}T)}\right] \qquad (12)$$

Lu (*10*) derived a rate expression equivalent to Equation (12) for an irreversible reaction, while Seth and Ross (*16*) correlated their hematite reduction data by similar equations. Warner (*20, 21*) discussed the interacting effects of boundary-layer transport, diffusion through the reduced layer, and interfacial reaction. Warner's data on the reduction of hematite cylinders by hydrogen illustrated the influence of gaseous diffusion.

Packed-Bed Reduction

El Mehairy and Philbrook (*7*) showed that the overall isothermal reduction rate of a fixed bed of hematite particles under constant pressure drop depended on two variables: (1) The supply rate of the reducing gas. As indicated by the Carman-Kozeny equation, the mass velocity varies as the square of the particle diameter for the low Reynolds number and constant pressure drop which prevailed in their study. (2) The total interfacial area available for surface reaction. For the constant bed volume, this varies inversely with the particle diameter.

An optimum size for maximum reduction rate existed, because increasing the particle size would gradually change control from the rate of supply of reducing gas to the surface area available for reaction.

Barner, Manning, and Philbrook, (*2*) using a digital computer, predicted the optimum particle size which corresponded to the maximum conversion rate. Particle reduction rates were obtained from McKewan's correlation of isothermal single-particle data. Reduction was postulated to stop when the reducing gas concentration reached the equilibrium p_{H_2O}/p_{H_2} ratio for the ferrous oxide/iron reaction. The following simplifying assumptions were made: flat velocity profile, negligible temperature gradients, and negligible axial diffusion.

Spitzer, Manning, and Philbrook (*17*) extended Barner's work and considered all three reduction steps (hematite-magnetite, magnetite-wüstite, and finally to iron), thus permitting additional use of reducing gas beyond the equilibrium value of ferrous oxide-iron. Three theoretical cases were considered.

Dense Particle Model. This model allowed reaction to continue by the gaseous reduction of magnetite to wüstite when the gas concentrations were less reducing than the ferrous oxide-iron equilibrium value, and similarly by the gaseous reduction of hematite to magnetite when the gas was too lean to produce the lower oxide. Transport resistances were neglected and only one surface reaction was assumed to occur at a given time. The reducing potential of the surrounding gas determined which reaction occurred.

Porous-Particle Models. Here interdiffusion of reducing gases was not restricted to the outer reduced shell but was allowed to proceed further into the other oxide phases. Thus the reducing gas, while diffusing into the pellet, may produce layers of magnetite or wüstite and may be almost completely depleted at the hemetite-magnetite interface. However, the gaseous products diffusing outward may reoxidize any wüstite or iron layers formed. Thus, two cases were considered: (1) *porous model* "A": where reoxidation is fast enough to produce stepwise reduction of the entire pellet. (2) *porous model* "B": where reoxidation is slow enough to be neglected and hence concentric cores of all phases will proceed inward by direct chemical reaction at the respective interfaces.

SINGLE-PARTICLE REDUCTION EXPERIMENTS

Equipment

The spring-type, thermogravimetric apparatus, which is shown schematically in Figure 1, consisted of a 42-mm. I.D. fused silica tube heated by an electric furnace. Furnace temperature was controlled with a chromel-alumel thermocouple situated between the silica tube and the furnace lining. The ore sample was placed in a wire basket which was attached to a nichrome spring by a fine chain. In turn, the spring was suspended from the top of the silica tube. The reducing gas flowed upward and was thereby heated by the furnace, then passed the ore basket and finally was let out of the silica tube through an opening just above the furnace. A second chromel-alumel thermocouple measured the temperature just below the ore sample. The spring was kept cool by forcing a cold stream of nitrogen around it. Spring extensions were followed with a cathetometer capable of reading extensions to 0.001 in., that is, to 0.01 g.

Procedure

The ore particle was weighed, placed in the basket, introduced into the furnace, and heated to the desired temperature. The cathetometer was adjusted to a mark on the spring. Then

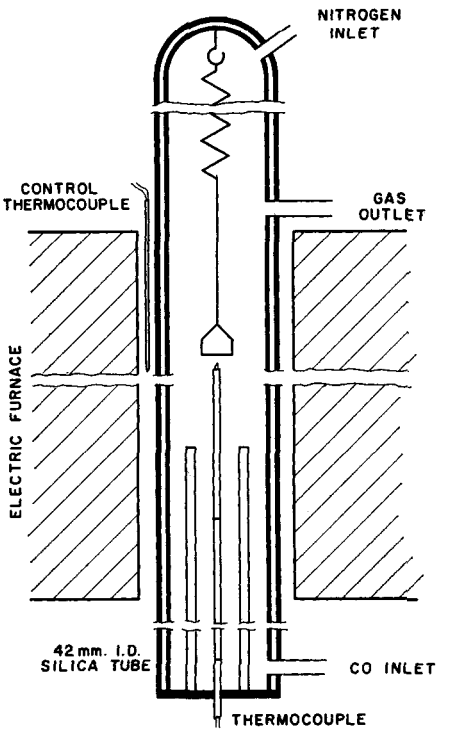

Fig. 1. Single-particle reduction equipment.

the reducing gas was passed at a metered rate through the silica tube while the cool nitrogen flowed downward. The weight loss was measured by following the decrease in extension of the spring.

Raw Materials

Vermilion ore particles and reagent grade ferric oxide spheres were used throughout. The ore was first crushed, sieved, calcined at 950°C. for 6 hr. in an electric furnace, and then sieved again before being used. The ore had the following analysis:

	Untreated ore	Treated ore
Iron	62%	64%
Phosphorus	0.1%	—
Manganese	0.07%	—
Silica	6.0%	4.65%
Alumina	2.7%	—
Water	—	0.033%

Results and Discussion

The scope of the single-particle data is:

Ore particle size	8.7 mm.
Hematite spheres	10 ± 1 mm. in diameter
Carbon monoxide flow rate	0.63 to 1 g./(sq.cm.)(min.)
Time of reduction	up to 90 min.
Fractional reduction	0 to 100%
Porosity of ore particles	1 to 18%
Porosity of hematite spheres	16 to 22%
Temperature	820° to 920°C.

Although cracking was observed in both partially reduced single particles and those reduced in packed beds, it was more pronounced in single-particle runs. In the later stages of reduction, the reaction rate decreased markedly, and sometimes the process stopped entirely. This effect was more pronounced the higher the carbon monoxide content of the reducing gas. This may be explained by increased carburization of the iron shell, thus forming austenite in place of part or all the ferrite. The resulting recrystallization could well aid, if not induce, cracking. Sintering of the outer shell could explain the observed decreases in the reaction rate. However sintering involves reduction in porosity of the iron shell and hence a net decrease in volume of the iron phase. It is therefore reasonable to expect the space occupied by the original hematite to be filled by a more massive iron phase, that is, closer to theoretical density, plus gross fissures or cracks rather than by an iron sponge with half its volume as widely distributed small pores. Unfortunately the above explanations are closer to postulations than proven facts.

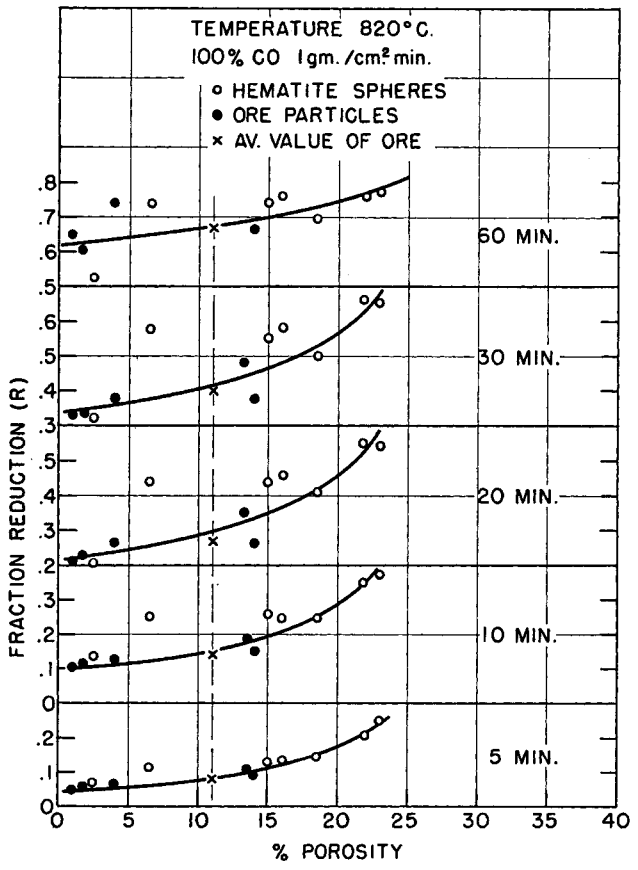

Fig. 2. Single-particle reduction data at 820°C.

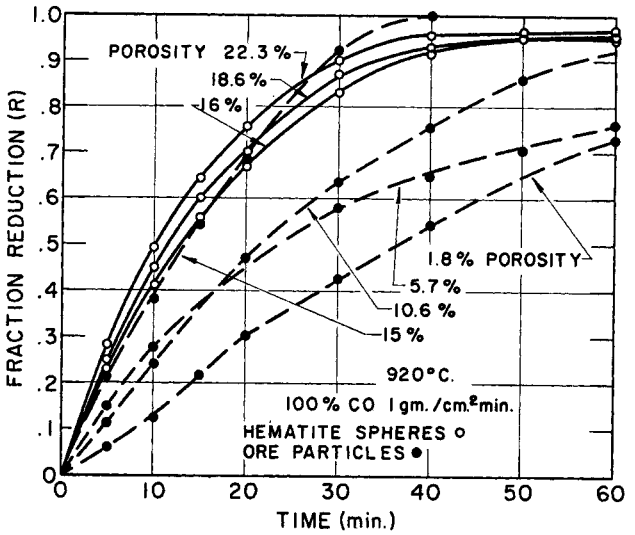

Fig. 3. Fractional reduction-time curves for single particles.

Apparent particle porosities were observed to increase from 10.6 initially to 40% after 90 min. of reduction at 920°C. Sintering of the entire shell of reduced iron would decrease the apparent particle porosity; however, the increase in porosity could be explained by the higher true density of iron to that of hematite. In addition if the particle either retained its original shape or underwent swelling during reduction, then the oxygen weight loss must produce a decrease in apparent particle density. The reduction rate could be decreased markedly by the sintering of a very thin layer of iron.

Reproducibility of results for single particles was poorer than for fixed beds. Irreproducibility resulted from the wide dissimilarities in shape, purity, and porosity among different particles and from variations in cracking and sintering patterns during reduction. Individual particle variations were hidden in packed-bed runs because several hundred particles were used at a time. Packed-bed weight losses were reproducible within ± 2% compared with ± 7% for single hematite spheres. Reproducibility in ore particle runs was still poorer owing to the difficulty of obtaining particles of identical weight, shape, and porosity.

Figure 2 shows typical reduction data for both ore particles and hematite spheres of different porosities as a function of time. Some scatter was observed even at the beginning of reduction when cracking and sintering effects were minimized. In the later stages of reduction the scattering became more pronounced due to nonuniform cracking and/or sintering of the particles. This illustrated the difficulty of correlating porosity and reducibility (measured as fractional reduction rate). Figure 3 shows typical variations of the fractional reduction with time for hematite spheres and ore particles at 920°C. To minimize the variation in ore particle results, the average

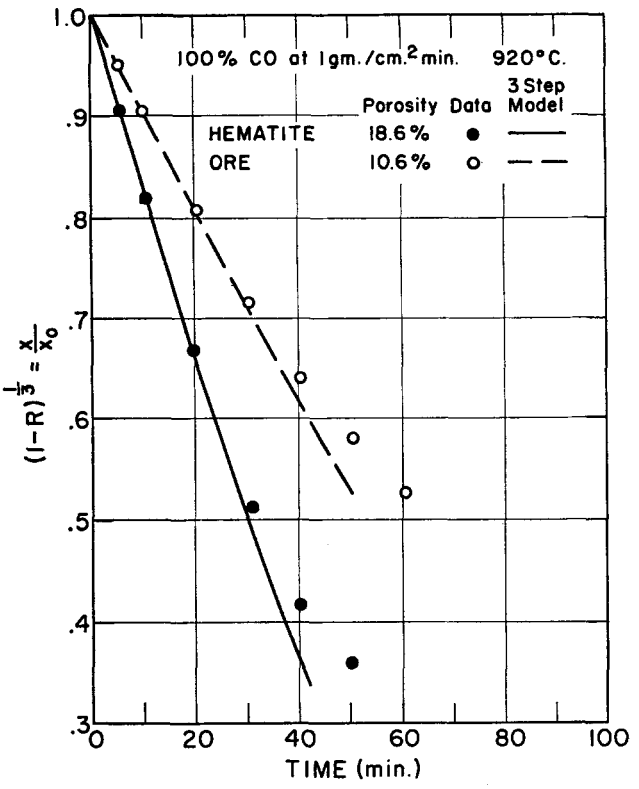

Fig. 4. Shell penetration rates for single particles with carbon monoxide.

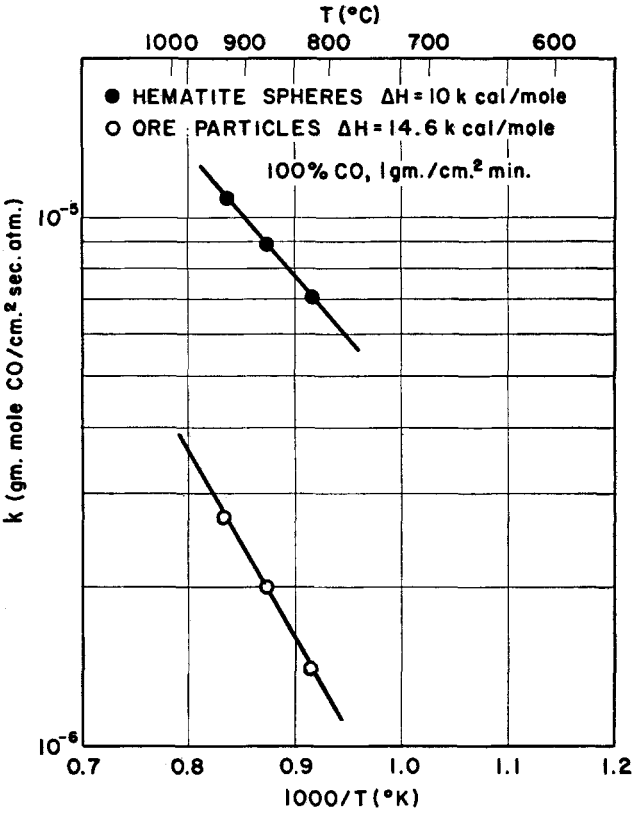

Fig. 5. Temperature coefficients for single-particle rate constants.

of values for several ore particles was used. Figure 4 shows the penetration (x_i/x_o) of the reduced shell, as computed from the weight loss, with time. The data were now fitted to the general three-step model as follows: the boundary-layer transfer coefficient h was first estimated with the Steinberger and Treybal formula (*18*). The diffusion resistance was assumed negligible during the first 5 min. of reduction and, therefore, Equation (10). Equation (10) may be simplified by omitting the shell diffusion resistance, that is, the

$$\left\{1-3\left(\frac{x_i}{x_o}\right)^2+2\left(\frac{x_i}{x_o}\right)^3\right\} x_o/6(D_{\text{eff}}/\mathcal{R}T)$$

term. The kinetic constant for this model was then determined by fitting the experimental data of the first 5 min. of reduction to this simplified form of Equation (10). The experimental effective diffusivity was then determined by trial until a single value yielded a close fit. No attempt was made to fit data taken during the later stages where sintering effects were considerable.

Figure 5 plots the kinetic constants for three-step model against the reciprocal of the absolute temperature, thus yielding the temperature coefficients as shown in Table 1. Differences between values for the ore particles and hematite spheres may be attributed to differences in the area available for reaction and to impurities. Reported kinetic constants depend on the actual surface area exposed to reaction rather than the theoretical spherical area ($4\pi x_i^2$).

Table 1 also presents the diffusivities obtained by fitting the data with the three-step model. The fitted diffusion coefficients for hematite spheres vary uniformly with temperature, while those of the ore particles show more scatter. This may be due to the greater variation in shape and purity among the ore particles. These fitted values are compared with the binary carbon monoxide-carbon dioxide diffusivities as estimated from Gilliland's equation and with the theoretical effective diffusivities as calculated from $D_{\text{theo.}} = (D_{AB}\epsilon)/\delta$, (5) where δ was set equal to 2 (22). Good agreement was observed between $D_{\text{theo.}}$ and $D_{\text{exp.}}$ at the low temperature of 820°C. [$D_{\text{exp.}} = 2(D_{\text{theo.}})$]. At the high temperature of 920°C., where sintering and cracking were appreciable, agreement between $D_{\text{theo.}}$ and $D_{\text{exp.}}$ was poor [$D_{\text{exp.}} = 10(D_{\text{theo.}})$].

It cannot be overemphasized that the fact that the three-step model can be fitted to the reduction data does

Table 1. Kinetic and Transport Coefficients for Single-Particle Data

Reduction temps. T, °C.	Kinetic constants $k_{\text{exp.}}$, g.-mole carbon monoxide/(sq. cm.)(sec.)(atm.) Ore	Hematite	Mass trans. coefficient h,* g.-mole carbon monoxide/(sq. cm.)(sec.)(atm.)	Binary diff. coefficient, D_{AB},† sq. cm./sec.	Shell diffusion coefficients, $D_{\text{theo.}}$,‡ sq. cm./sec. Ore	Hematite	Experimental shell diffusion coeff. $D_{\text{exp.}}$, sq. cm./sec. Ore	Hematite
820	1.4×10^{-6}	7.0×10^{-6}	6.7×10^{-5}	1.12	2.0×10^{-1}	2.5×10^{-1}	2.0×10^{-1}	2.8×10^{-1}
870	2.0×10^{-6}	9.0×10^{-6}	6.7×10^{-5}	1.14	2.2×10^{-1}	2.7×10^{-1}	1.5×10^{-1}	6.7×10^{-1}
920	2.7×10^{-6}	10.8×10^{-6}	7.0×10^{-5}	1.25	2.4×10^{-1}	3.0×10^{-1}	1.0×10^{-1}	11.4×10^{-1}

* h estimated from the Steinberger and Treybal formula.
† D_{AB} estimated from the Gilliland formula.
‡ $D_{\text{theo.}} = (\epsilon D_{AB})/\delta$.

not confer uniqueness or physical reality on the model. For example, the linear rate at which the unreduced core receded in the early stages of reduction indicated that these data could be fitted also by the single-step equation for interface reaction control. Obviously, this fit should not be interpreted to mean that boundary-layer transport offered no resistance. The boundary-layer mass transport coefficient was not infinite, as indicated by the magnitude of the estimated values (*18*) in Table 1.

FIXED-BED REDUCTION

Equipment

The flow diagram of the equipment is shown in Figure 6. The reducing gas (carbon monoxide) flowed from the storage cylinder through a pressure regulator; through a drying tower to a calibrated rotameter, the flow in which was controlled by a needle valve; and finally to the reducing capsule. Nitrogen gas was used to provide an inert atmosphere in the capsule while cooling the reduced bed and to displace air before admitting carbon monoxide, thus eliminating explosive mixtures. The nitrogen was passed over heated copper foil at 300°C. to remove any residual oxygen impurity. Anhydrous calcium sulfate was used as drying agent. The reduction capsule, which is shown in Figure 7, was made of type 304 stainless steel seamless pipe and contained a gas-preheating section which was fiilled with ½-in. ceramic pellets. The length of the preheater was designed so that the reducing gas could be heated to within 10°C. of the wall temperature if the gas mass velocity was less than 0.3 g. carbon monoxide/(sq. cm.)(min.) (*12*). The section enclosing the ore bed, which was supported by a stainless steel wire screen, was placed above the preheater section. A layer of refractory cement sealed the upper edge of this threaded joint, thus ensuring no loss of the premeasured reducing gas before it flowed through the bed. The cap was secured in place over the fixed bed by eight bolts. A small hole in the cap permitted direct measurement of the bed temperature with a chromel-alumel thermocouple. Two tappings, one just before the ore bed and the other just above it, permitted the pressure drop across the bed to be measured by an inclined manometer with a range of 0 to 1 in. of water in graduations of 0.01 in.

The gases leaving the bed were passed through a Ranarex gas analyzer before being burned. This Ranarex reading enabled the calculation of the carbon dioxide content within ± 2%.

Procedure

The ore bed was weighed and mounted on the capsule, which was then put in the furnace. A stream of nitrogen was passed through the ore bed while it was heated. When the temperature reached the desired value, the carbon monoxide was turned on at a premeasured constant flow rate and passed through the bed for the desired time. During reduction, the gases leaving the bed were passed through the Ranarex gas analyzer, which was read periodically. At the end of a run, the bed was flushed with nitrogen for a few minutes and the capsule removed from the furnace. The nitrogen stream was kept flowing through the capsule until it cooled down to room temperature, at which time the reduced bed was weighed to get the weight loss and fractional reduction.

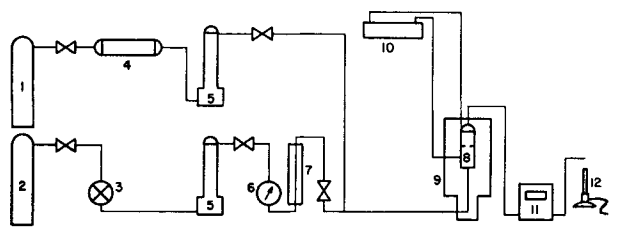

Fig. 6. Flow sheet of reduction equipment.

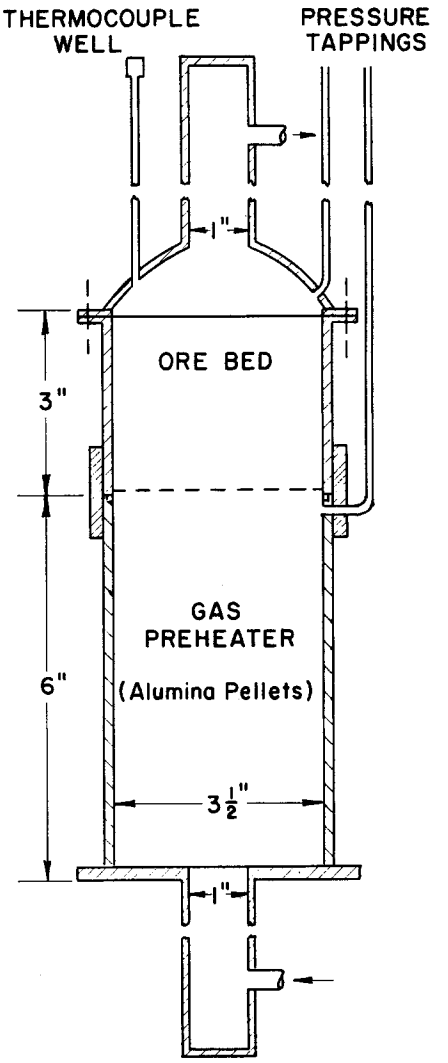

Fig. 7. Reduction capsule.

Results and Discussion

The scope of the present packed-bed work is:

Average ore particle porosity	10.6%
Average ore particle size	8.7 to 7.14 mm.
Bed height	7.8 cm.
Bed diameter	8.9 cm.
Bed void fraction	0.5
Temperature	550° to 920°C.
Reduction time	20 to 90 min.
Fractional reduction	up to 75%
Gas flow rate	0.3 to 0.4 g./(sq.cm.)(min.)

Figure 8 shows the variation in exit gas composition with time for two temperatures, 760° and 920°C., and three particle sizes, 3.1, 6.0, and 8.7 mm. High temperature results were emphasized because carbon deposition was appreciable in experiments carried out below 760°C. Initially the carbon dioxide content in the exit gas was greater than the ferrous oxide-iron equilibrium value. These high carbon dioxide contents indicated that reduction of fresh ore particles was considerably faster at the beginning and that carbon monoxide was used to form some magnetite and some wüstite when the reducing gas was too lean to produce iron. Reduction rates decreased rapidly after about 25 min. The pressure drop across the

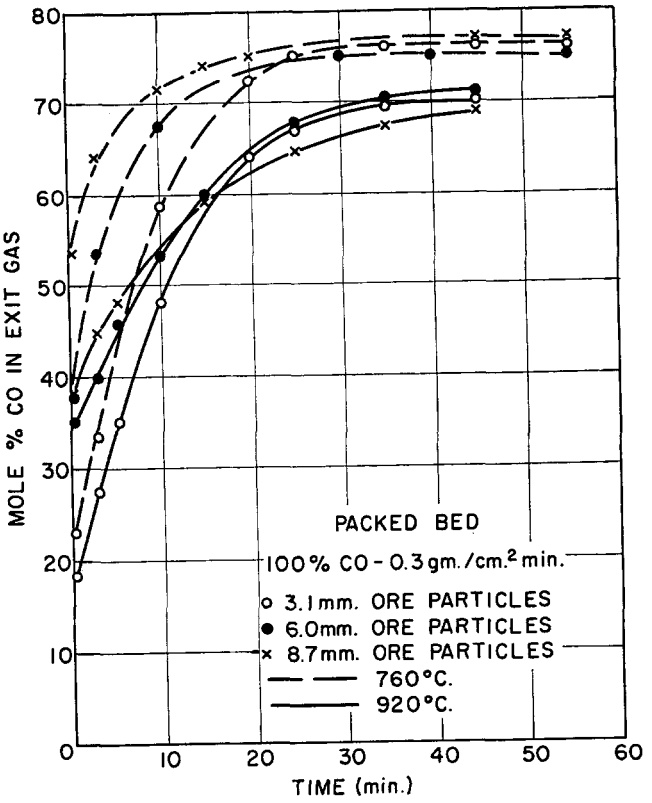

Fig. 8. Packed-bed exit gas compositions.

bed increased during reduction, for example, a 50% increase after 30 min. reduction at 870°C. was typical. This increase could be attributed, with the Carman-Kozeny equation, to a decrease in interparticle void fraction from 50 to 46%, and thus could illustrate swelling phenomenon frequently associated with hematite reduction.

Predictions of Fixed-Bed Reduction Rates

Barner's method (*1*, *2*) of predicting fixed-bed reduction rates was modified to include the general, three-step, single-particle rate expression, that is, Equation (10). Figures 9 and 10 present the resulting predictions of overall bed reduction rates and exit gas composition and compare them with the experimental data. The modified program used three rate coefficients: h, $D_{exp.}$, and $k_{exp.}$. The boundary-layer transport coefficient h was reestimated for the packed ore bed (3), while $k_{exp.}$ and $D_{exp.}$ were evaluated as described previously from the single-particle data and Equation (11). Predictions of the reduction rates agreed closely with the data, but appreciable deviation was observed between the predicted and experimental exit gas compositions. This failure to predict exit gas compositions, especially the initial values, suggested that Barner's simplifying assumptions were inadequate. Hematite reduction could not be considered as merely the reduction of wüstite to iron, and reduction should not be assumed to stop when the carbon monoxide content approached the ferrous oxide-iron equilibrium value.

Accordingly, Spitzer's dense-pellet model (*17*) was not modified. Spitzer's model treats the Fe_2O_3-Fe_3O_4, Fe_3O_4-FeO, and FeO-Fe steps separately and therefore involves seven rate coefficients: h for the boundary layer and a separate pair of D_{eff} and k for the iron, wüstite, and magnetite layers. Unfortunately all of these seven rate coefficients could not be obtained from independent sources and hence some curve fitting to the fixed-bed data was required. In order to reduce computer time the boundary-layer transfer coefficient was omitted. This simplification reduced computation time considerably and separate calculations showed that including h as the seventh constant did not improve the fit significantly. Six constants still remained to be evaluated:

$$3\,Fe_2O_3 + CO \overset{k_1,D_1}{\rightleftharpoons} 2\,Fe_3O_4 + CO_2$$

$$Fe_3O_4 + CO \overset{k_2,D_2}{\rightleftharpoons} 3\,FeO + CO_2$$

$$FeO + CO \overset{k_3,D_3}{\rightleftharpoons} Fe + CO_2$$

Transport coefficients for the iron layer D_3 and k_3 were obtained by setting $D_3 = D_{exp.}$ and $k_3 = k_{exp.}$. In turn, $D_{exp.}$ and $k_{exp.}$ were obtained as previously described from the single-particle data. The effective diffusivities of the wüstite and magnetite layers were estimated with the expected variation of diffusivity with void fraction:

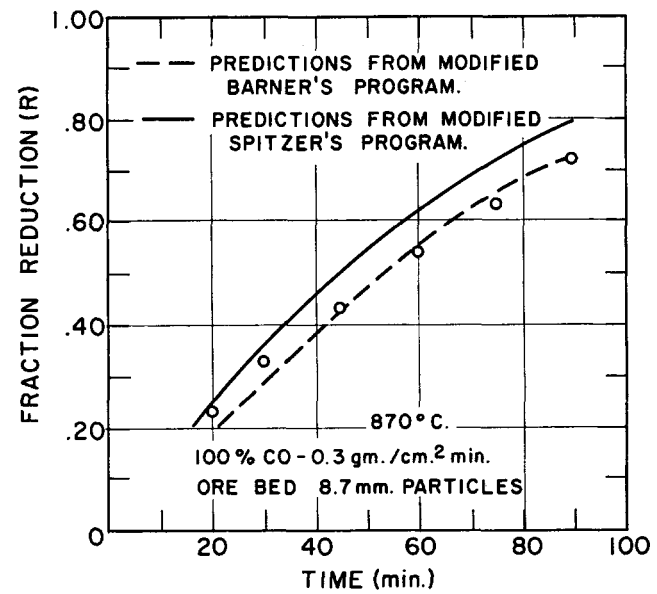

Fig. 9. Comparison of packed-bed reduction rates with Barner's and Spitzer's predictions.

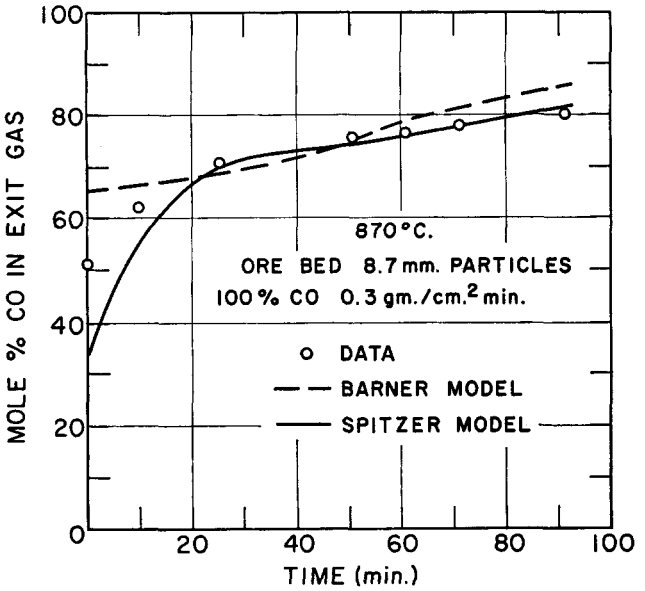

Fig. 10. Comparison of packed-bed exit gas compositions with Barner's and Spitzer's predictions.

$$D_1/\epsilon_1 = D_2/\epsilon_2 = D_3/\epsilon_3$$

The void fractions were computed from the theoretical densities of hematite, magnetite, wüstite, and iron and the known initial porosity of the hematite particle. Finally k_1 and k_2 were varied independently until a good fit of the experimental reduction rates and exit gas compositions was obtained.

Figures 9 and 10 compare the fixed-bed data with the predictions resulting from Spitzer's modified model. The reported predictions were obtained with

$$k_{exp.} = k_3 = 1.5\ k_2 = k_1$$

Again the predicted bed reduction rates agreed quite closely with the experimental rates, while significant deviation was observed between the predicted and experimental exit gas compositions. However, Spitzer's model, with its six constants, was able to reproduce the general shape of the exit gas composition if not the observed values.

Many explanations could be found for the deviations between the packed-bed data and the model predictions. The behavior of each particle in the packed bed was assumed to be similar to its behavior if reduced individually. Particle interactions, that is, the effect of the neighboring particles on the mass transfer to and from any one particle, have not been included. Care was taken to pack the bed uniformly, but the absence of channeling of the rising reducing gases with the resulting local hot and cold spots could not be guaranteed. Isothermal reduction was assumed but temperature fluctuations, while kept small (less than 10°C.), could not be eliminated. Even the partial agreement of multistep reaction models with single-particle results does not exclude the argument that these models may not be the correct ones, or if they are, the complete set of rate constants and material properties may not yet be correctly known. Deviation from the experimental results may also be attributed to cracking and sintering. None of the models considers these complications.

ACKNOWLEDGMENT

This report is based upon a thesis submitted by M. A. Osman in partial fulfillment of the requirements for the degree of Doctor of Philosophy in Chemical Engineering.

Financial support of this research by the American Iron and Steel Institute is gratefully acknowledged.

The United Arab Republic is thanked for granting Dr. Osman an extended leave of absence and for supporting his study at the Carnegie Institute of Technology.

The authors thank Robert Spitzer for his help in modifying his reduction models and in writing the computer programs.

NOTATION

A = surface of particle or pellet, sq. cm.
D = gas diffusivity, sq. cm./sec.
D_{AB} = binary gas diffusivity as estimated from the Gilliland formula, sq. cm./sec.
d_O = oxygen content of pellet, g. oxygen/cc.
h = mass transfer coefficient for boundary layer surrounding particle (g.-moles carbon monoxide/(sq. cm.)(sec.)(atm. carbon monoxide)
K_e = equilibrium ratio of carbon dioxide to carbon monoxide for wüstite-iron equilibrium at reaction temperature
k = surface reaction rate constant, g. atoms of oxygen removed from oxide core/(sq. cm.)(sec.)(atm. carbon monoxide)
M = molecular weight
n = g.-moles
P = total pressure of reducing gas, atm.
R = fractional reduction, oxygen removed/total removable oxygen
$\mathcal{R}$ = gas constant 82.03 (atm.)(cc.)/(g.-mole)(°K.)
t = time, sec.
W = mass, g.
X = fictitious boundary-layer thickness, cm., in Equation (14)
x = radial distance from center of particle, cm.
y = mole fraction

Greek Letters

δ = tortuosity factor
ϵ = porosity of reduced shell

Subscripts

eff = effective value in which combined effects of shape, cracking, porosity, and possibly sintering are included
exp. = value obtained by fitting model to data
f = bulk gas phase property
i = value at ferrous oxide-iron interface
O = oxygen weight loss
o = value at external surface of particle
1,2,3 = magnetite, wüstite, and iron layers, respectively

Superscripts

$'$ = reducing gas, carbon monoxide
$''$ = product gas, carbon dioxide

LITERATURE CITED

1. Barner, H. E., M.S. thesis, Carnegie Inst. Technol., Pittsburgh, Pa. (1962).
2. Barner, H. E., F. S. Manning, and W. O. Philbrook, *Trans. Am. Inst. Mech. Engrs.*, **227**, 897 (1963).
3. Bird, R. B., W. E. Stewart, and E. N. Lightfoot, "Transport Phenomenon," 2 ed., p. 679, Wiley, New York (1962).
4. Bitsianes, G., and T. L. Joseph, *Trans. Am. Inst. Mech. Engrs.*, **197**, 1641 (1953).
5. Carman, P. C., "Flow of Gases Through Porous Media," p. 46, Butterworth, London (1956).
6. Edstrom, J. O., *J. Iron Steel Inst.*, **175**, 289 (1953).
7. El-Mehairy, A. E., and W. O. Philbrook, "Proc. Blast Furnace, Coke Oven, and Raw Materials Committee," Vol. 20, p. 280, Am. Inst. Mech. Engrs., New York (1961).
8. Hougen, O. A., and K. M. Watson, *Ind. Eng. Chem.*, **53**, 529 (1943).
9. Kawasaki, E., J. Sanscrainte, and T. J. Walsh, *A.I.Ch.E. J.*, **8**, 48-52 (1962).
10. Lu, W. K., *Trans. Am. Inst. Mech. Engrs.*, **227**, 203 (1963).
11. McCabe, W. L., and J. C. Smith, "Unit Operations of Chemical Engineering," McGraw-Hill, New York (1956).
12. McAdams, W. H., "Heat Transmission," 3 ed., p. 291, McGraw-Hill, New York (1954).
13. McKewan, W. M., *Trans. Am. Inst. Mech. Engrs.*, **218**, 2 (1960).
14. McKewan, W. M., and N. D. Smith, "Blast Furnace, Coke Oven and Raw Materials," Vol. 21, pp. 3-13, Am. Inst. Mech. Engrs., New York (1962).
15. Osman, M. A., M.S. thesis, Carnegie Inst. Technol., Pittsburgh, Pa. (1964).
16. Seth, B. B. L., and H. U. Ross, *Trans. Am. Inst. Mech. Engrs.*, **233**, 180 (1965).
17. Spitzer, R. H., F. S. Manning, and W. O. Philbrook, "Process Simulation in Iron and Steelmaking," Gordon and Breach, New York, in press.
18. Steinberger, R. L., and R. E. Treybal, *A.I.Ch.E. J.*, **6**, 226 (1960).
19. Themelis, N. J., and W. H. Gauvin, *Trans. Am. Inst. Mech. Engrs.*, **227**, 290 (1963).
20. Warner, N. A., *ibid.*, **230**, 163 (1964).
21. ———, *Australian Inst. Min. Met. Proc.*, **210**, 31 (1964).
22. Wheeler, A., "Advances in Catalysis," Emmett, ed., Vol. III, p. 266, Academic Press, New York (1951).

Manuscript received July 16, 1965; revision received January 14, 1966; paper accepted January 17, 1966.